ICAM
10th International Congress for Applied Mineralogy
Trondheim 2011

# SYSTEMATIC REE PARTITIONING IN CUBO-DODECAHEDRAL FLUORITE FROM BELGIUM REVEALED BY CATHODOLUMINESCENCE SPECTRAL IMAGING AND LASER ABLATION-ICP-MS

Jean-Marc Baele[1]*, Laurence Monin[2], Jacques Navez[2], Luc André[2]

[1]Department of Geology, Faculty of Engineering, University of Mons, 9 rue de Houdain, B-7000 Mons, Belgium

[2]Division Mineralogy-petrography-geochemistry, Department of Earth Sciences, Royal Museum for Central Africa, 13 Leuvensesteenweg, B-3080 Tervuren, Belgium

**Abstract**

Geochemistry of the rare earth elements (REE) in fluorite is widely used in ore geology. However, bulk analysis may be biased by compositional heterogeneity in crystals. Here we report a systematic REE partitioning in cubo-dodecahedral fluorite crystals from Belgium using cathodoluminescence (CL) spectral imaging and laser ablation-inductively coupled plasma-mass spectrometer (LA-ICP-MS) analysis. The light REE (LREE) are markedly enriched, and heavy REE (HREE) depleted in the |110| sector relative to the |100| sector. The partition coefficient $K_{|110|/|100|}$ is >10 for LREE and <1 for HREE. Very contrasting REE patterns and ratios are thus recorded from the same crystal. CL can be used for imaging compositional heterogeneities since REE are known CL activators in fluorite. However, CL imaging is found of limited application when the REE lines are masked by the strong $Eu^{2+}$ emission. Spectral imaging of other REE lines solved this problem by producing sharp and contrasted compositional images.

**Keywords**: REE, fluorite, cathodoluminescence, LA-ICP-MS, Belgium

## 1 INTRODUCTION

Trace-elements geochemistry provides important information for research in ore geology. The rare earth elements (REE) in fluorite have long been used as petrogenetic indicators since fluorite is a common gangue mineral in many deposits (e.g., [1] and references therein). Chondrite or shale-normalized REE patterns, REE anomalies and ratios such as Tb/Ca-Tb/La [2] are the most preferred indicators in these studies. REE patterns are generally interpreted in terms of general REE abundance and anomalies in REE that are commonly oxidized ($Ce^{4+}$) or reduced ($Eu^{2+}$) and hence behave differently than $REE^{3+}$ in geochemical systems. Besides Ce and Eu anomalies, the overall shape of REE patterns reflects fractionation between light REE (LREE, from La to Eu) and Heavy REE (HREE, from Gd to Lu, including Y).

Research on REE in fluorite recently beneficiated from spectacular advances in microsampling techniques such as laser ablation systems, which can feed an inductively coupled plasma-mass-spectrometer (ICP-MS) for local trace-element analysis at ~ppb levels with a spot size of a few tens of micrometers [1, 3, 4]. Other advanced techniques such as synchrotron X-ray fluorescence microanalysis (SXRFMA) have also been used to investigate compositional heterogeneities in fluorite [5, 6]. These studies showed important partitioning of the REE among symmetrically nonequivalent sectors and various partition coefficients were reported.

* Correspondence to: jean-marc.baele@umons.ac.be

Maarten A. T. M. Broekmans (ed.), *Proceedings of the 10th International Congress for Applied Mineralogy (ICAM)*, DOI: 10.1007/978-3-642-27682-8_4,

However, no systematic trend was observed for the most common sectors in fluorite that correspond to the growth of the cube sector |100| and the dodecahedron sector |110|.

Here we report a systematic partitioning of REE between |110| and |100| sectors in fluorite from several deposits in South Belgium. Preferential incorporation of LREE into the |110| sector commonly exceeds 1 order of magnitude relative to the |100| sector. As suggested by Bosze and Rakovan [5], these results have important implications on the use of REE analysis in bulk fluorite for petrogenetic research. We suggest further caution in using cathodoluminescence for detecting compositional heterogeneities in fluorite since the REE emission lines can be masked by the strong $Eu^{2+}$ emission. To overcome this, we develop a simple method based on cathodoluminescence spectral imaging.

## 2 MATERIALS AND METHODS

### 2.1 Samples and preparation

*Sample description*

Fluorite samples were collected in South Belgium and nearby localities in France where small replacement, vein and karst-like deposits occur in Palaeozoic carbonate rocks [7]. Five sample localities were considered among a total of nine for this contribution: Han-sur-Lesse (Han), Lavaux-Sainte-Anne (Lav), Matagne-la-Grande (Mat), Rancennes (Ran), and Seilles (Sei). Samples from deposits that are no longer accessible were kindly provided by private collectors. The fluorite samples consist of millimeter to centimeter crystals or aggregates of various colors (dark to light purple, green, yellow, or colourless). The investigated crystals exhibit the cube {100} faces with variable development of the rhombododecahedral {110} faces. Color variation in single crystals is common in both growth and sectoral zoning. It was observed that the blue color is restricted to the cube sector |100| and that the purple color is often enhanced in this sector.

*Preparation*

Fluorite is a highly cleavable mineral. Hence, the samples were firstly embedded in cold-mounting epoxy-resin to minimize damages during processing. When possible, crystallographically orientated sections were prepared based on the careful examination of the external morphology of the crystals. Standard (30 μm) thin-sections were too thin for microsampling with the laser ablation system as well as for the observation of color variations, which became too faint to be discernible. Therefore, it was decided to make thick sections of a few hundredths of micrometer to a few millimeter thick. Section processing included sawing, grinding with a SiC (grid 800) aqueous suspension, and three-step polishing on cloths using successively 6, 3, and 1 μm diamond gels.

### 2.2 Analytical methods

*Cathodoluminescence (CL)*

Cathodoluminescence analysis was performed at Geology Deptartment, UMons, using a CITL Mk5 cold-cathode CL unit operating at maximum 30 kV and 1 mA of beam voltage and current, respectively. Typical operating conditions for the fluorite analysis were 10–15 kV and 500 μA. The CL unit was mounted on a Universal-R Zeiss optical microscope.

Spectroscopic measurements were carried out using a CITL COS8200 optical spectrometer which collects light with a 100 μm optical fibre and scatters it with a 300 grooves/mm diffraction grating. Spectra are recorded by a Peltier-cooled charge coupled device (CCD) camera consisting of a linear array of 2048 pixels of 14 × 100 μm in size each. The spectral resolution and range are ~3.7 nm and 350–1100 nm, respectively. The spot size for spectral analysis is about 35 μm. The spectra were not corrected for system

response, which is not critical for the identification of the sharp REE emission lines and mutual comparison of spectra. They were corrected for background emission (stray light).

Spectral imaging was achieved by inserting optical passband filters in front of the tube lens of the CL microscope. Spectral images were recorded with a high-sensitivity Peltier-cooled CCD camera (Lumenera Infinity3). The same camera was used for both total and spectral CL imaging and typical exposure times for these observation modes were <1s and a few seconds, respectively. Both narrow and broad band filters were utilized. Their choice is a trade-off between spectral selectivity and sensitivity. Commercially available interference passband filters have a filtering peak with a full width at half maximum height of about 10 nm for narrow band filters and a few tens of nanometer for broad band filters. Their central filtering wavelength (CFW) was chosen as close as possible to the characteristic REE emission which has minimum interference with other emissions. The following CFWs were selected : 420 nm for $Eu^{2+}$, 671 nm for $Dy^{3+}$, 640 nm for $Sm^{3+}$, and 880 nm for $Nd^{3+}$.

*Laser ablation-inductively coupled plasma-mass spectrometer analysis (LA-ICP-MS)*

The LA-ICP-MS measurements were performed at Geology and Mineralogy Department, Royal Museum for Central Africa. A New-Wave UP-193 FX fast excimer (193nm) laser coupled with a Thermo Scientific X-Series2 quadrupole ICP-MS was used. The laser was run at 50 Hz and an energy fluence of 10 J/cm$^2$ for a 100-µm spot size. He gas at a flow rate of 0.65 l/min was flushed into the ablation cell and was mixed after the cell with Ar carrier gas at a flow rate of 0.76 l/min. $^{43}Ca$ was used as internal standard for correcting instrumental drift and ablation rate. The NIST SRM 614 and 612 were used as external standards and were measured frequently during the course of the analyses. The precision at 1 sigma level on the NIST SRM 612 is below 10% RSD and the detection limits are 20 ppb for Nd and between 4 and 10 ppb for other REE.

## 3 RESULTS

### 3.1 Cathodoluminescence analysis

All fluorite samples exhibited a blue cathodoluminescence. Many regions examined were homogeneous while other regions showed noticeable variations in intensity and color consistent with growth and sectoral zoning or healed microfractures (Figure 1). The crystals we studied may display one of these two different types of CL emission (homogeneous or heterogeneous) across their entire section. Typically, fluorite crystals that deposited in fractures and cavities showed a heterogeneous CL emission in their central region, which becomes gradually homogeneous outwards (Figure 2). Greenish-blue and pinkish- to light-blue CL colors are characteristic of the |100| and |110| sectors, respectively. As observed by Dickson [8], virtually all the fluorite samples developed a heterogeneous, semi-permanent purple color due to electron bombardment. It was observed that the |100| sector developed a significantly darker color than the |110| sector, which was useful in revealing sectoral zoning in colorless fluorite.

Spectral analysis showed a systematic strong broad band emission in the blue region at ~420 nm (Figure 3). This emission is attributable to both crystal defects (intrinsic luminescence) and $Eu^{2+}$ activation (extrinsic luminescence) (peak assignment after [9, 10]). Many spectra revealed additional sharp lines that are characteristic of $REE^{3+}$ activation : $Dy^{3+}$ at 575, 670, and 760 nm ; $Sm^{3+}$ at 570, 605, and 640 nm ; $Tb^{3+}$/$Er^{3+}$ at 540 and 550 nm, and $Nd^{3+}$ at ~870 nm. In REE-activated samples, the characteristic emissions of HREE (Dy and Tb/Er) dominate over LREE in the |100| sector and the reverse is observed in the |110| sector (Figure 1). This is consistent with the observed color variations in CL imaging since strong emissions are produced in the green region by Dy and Tb/Er and in the red region by Sm. This trend is still observable in

spectra from weakly REE-activated fluorite but is difficult to detect in CL imaging because it is masked by the strong intrinsic/$Eu^{2+}$ emission in the blue region. In contrast, the spectra collected perpendicular to growth zoning in a given sector yielded consistent variations of all the $REE^{3+}$ lines.

Spectral imaging aimed at mapping the following CL activators: (1) intrinsic/$Eu^{2+}$ (filtering wavelength = 420 nm), (2) $Sm^{3+}$ (640 nm), (3) $Dy^{3+}$ (671 nm), and (4) $Nd^{3+}$ (880 nm). The resulting spectral images on a crystal section exhibiting heterogeneous CL due to growth and sectoral zoning are shown in Figure 1. Sector assignment in this sample was based on the observation of its external cubo-dodecahedral morphology. The brightness in a given spectral image is proportional to the intensity of CL activation. The images in Figure 1 clearly show that the |100| sector is highly activated by Dy while it is weakly activated by Sm and Nd. The reverse is observed in the |110| sector. Comparing Nd and Dy spectral images, which seem to result from a mere brightness inversion, one can document a spectacular partitioning of REE activation across symmetrically nonequivalent sectors. An example with fluorite exhibiting homogeneous CL (or nearly) is given in Figure 2. In this example, only a faint growth zoning is visible in the central region of the crystal, which is enriched in REE relative to the outer rim (see next section). In this sample, spectral imaging of the Nd line revealed the same contrasted distribution of REE activation between the |100| and |110| sectors in addition to its fading out from the crystal centre outwards. Nd spectral images are usually brighter, more contrasted, and sharper than the others. Various crystal textures, such as the fine details of growth zoning, are enhanced in these images. Nd images also revealed a dark vein-like pattern branching to small scattered |100| domains ("subsectors") in the |110| sector of some samples (Figure 1). Furthermore, the morphological change as fluorite crystals were growing can be easily reconstructed by spectral imaging. It was noticed that many samples showing the cube on their external morphology are in fact overgrowths of earlier formed cubo-dodecahedral crystals.

### 3.2 LA-ICP-MS analysis

The analytical results that are presented here are representative of one sample per sample locality (two samples for locality "Mat"). Most of them are spot analysis along profiles extending across 1 to 3 cm wide crystal sections. The profiles were established in sectors that were either visible from macroscopically visible crystal faces or revealed by cathodoluminescence spectral imaging.

Chondrite-normalized patterns of the |110| sector show a strong enrichment in LREE and depletion in HREE relative to the |100| sector (Figure 4). All samples follow this trend and patterns from the same sector of different samples are strikingly similar, except for the general REE abundance and perhaps Ce anomaly, which is slightly negative in sample "Sei". Only a few patterns plot otherwise but they correspond to analyses in heterogeneous |110| sectors and therefore represent a mixed influence of the |100| and |110| sectors. An example of analysis in such a crystallographically heterogeneous sector can be seen in Figure 1. Samples "Han" and "Lav" yield REE patterns consistent with the decrease in REE activation from their centre outwards, which was revealed by CL analysis. These samples exhibit a general decrease in REE abundance but no substantial change in the shape of the pattern.

In the Tb/La-Tb/Ca diagram [2], virtually all the analyses representative of the |100| sector plot in the "sedimentary" field while that in the |110| sector plot in the "hydrothermal" field (Figure 5). Variations in Tb/La from these sectors are up to 2 orders of magnitude in the same sample.

The partition coefficient $K_{|110|/|100|}$, that is, the enrichment factor of the REE in the |110| sector relative to the |100| sector, was determined in sample "Mat" based on analyses in coeval regions (i.e., a given growth zone) from adjacent sectors. Analyses were performed in three different growth zones of the crystal.

The results (Table 1) show a continuous decrease of $K_{|110|/|100|}$ from 20 to 1 for LREE (La to Gd) and a stabilization around 0.70 for HREE.

## 4 DISCUSSION

Our results demonstrate a spectacular partitioning of trace elements into two extremely common sectors in fluorite (|100| and |110|). Analyses of bulk fluorite may therefore be strongly biased as they would primarily reflect an average (with *a priori* unknown weighting factors) of two extreme situations in the crystal. The fluorite from South Belgium showed a variable development of the {100} and {110} crystal faces, even in crystals from the same deposit or hand sample. In addition, the relative proportion between the |100| and |100| sectors was found variable form the centre of some crystals outwards. Therefore, the external morphology of a crystal cannot be extrapolated to its entire volume and careful investigation of sections is necessary to assess crystal heterogeneity. Our spectral imaging also indicated that macroscopically visible crystal faces may in fact be associated to crystallographically heterogeneous sectors, especially the |110| sector, which can contain numerous |100| subsectors. This is critical for microanalysis such as LA-ICP-MS or other similar techniques.

As suggested by Bosze and Rakovan [5], surface-structure-controlled processes would explain the partitioning in symmetrically nonequivalent crystal faces. It was indeed noticed that the {110} crystal face in our samples is often significantly rougher than the {100} face and this probably relates to the presence of |100| subsectors. The fact that the partition coefficient gradually decreases from La to Gd may be associated with the influence of the ionic radius of the $REE^{3+}$ substituting for $Ca^{2+}$ in the fluorite lattice.

A similar LREE enrichment and HREE depletion has been published by Smolyanskii et al. [6] in fluorite crystals from Nordvik (Russia). However, according to the authors, their crystals exhibited the |111| (octahedral) and |100| sectors. Tough their $K_{|111|/|100|}$ are very close to the $K_{|110|/|100|}$ we report here. Bosze and Rakovan [5] have studied a variety of different sectors in fluorite from Long Lake and Bingham (USA) but no systematic trend has been reported for the |100| and |110| sectors. However, they have mentioned in their publication a $K_{|100|/|110|}$ of 1.77 (i.e., $K_{|110|/|100|} = 0.56$) for Dy in a sample from Bingham, which is consistent with our results.

## 5 CONCLUSIONS

Cathodoluminescence spectroscopy and spectral imagaing and LA-ICP-MS analysis showed that fluorite crystals from South Belgium exhibit a marked compositional heterogeneity due to systematic partitioning of REE in the |100| and |110| sectors. LREE are preferentially incorporated in the |110| sector with a partition coefficient $K_{|110|/|100|}$ gradually decreasing from 20 to 1 from La to Gd. Conversely, HREE are depleted in this sector but to a lesser extent ($K \sim 0.7$). These results suggest caution when using bulk REE analysis as petrogenetic indicators since trace-element incorporation in fluorite is in part controlled by crystal growth factors. This can significantly bias the geochemical information carried by fluorite and lead to misinterpretation about its genesis or provenance. Cathodoluminescence can be used to detect compositional heterogeneities and assist microanalysis but sectoral zoning may be masked by the strong intrinsic/$Eu^{2+}$ blue emission of fluorite. Spectral imaging using a simple technique based on optical filters may overcome this by providing sharp and contrasted compositional images with respect to the REE.

## 6 ACKNOWLEDGMENTS

We are very grateful to Roger Leemans and Christophe Ottermans (CMPB Brussels), Guy Evrard (Grottes de Han associatione), and Thierry Mortier (La Malogne asbl) for providing some of the fluorite samples that were investigated in this study.

## 7 REFERENCES

[1] Schwinn, M and Markl, G (2002): REE systematic in hydrothermal fluorite. Chemical Geology (216): 225–248.

[2] Möller, P, Parekh, P, and Schneider, HJ (1976): The application of Tb/Ca-Tb/La abundance ratios to problems of fluorspar genesis. Mineralium Deposita (11): 111–116.

[3] Gagnon, JE, Samson, IM Fryer, BJ, and Williams-Jones, AE (2003): Compositional heterogeneity in fluorite and the genesis of fluorite deposits: insights from LA-ICP-MS analysis. Canadian Mineralogist (41): 365–382.

[4] Schönenberger, J, Köhler, J, and Markl, G (2008): REE systematic of fluorides, calcite and siderite in peralkaline plutonic rocks from the Gardar Province, South Greenland. Chemical Geology (247): 16–35.

[5] Bosze, S and Rakovan, J (2002): Surface-structure-controlled sectoral zoning of the rare earth elements in fluorite from Long Lake, New York, and Bingham, New Mexico, USA. Geochimica et Cosmochimica Acta (66): 997–1009.

[6] Smolyanskii, PL, Proskurnin, VF, and Bogomomlov, ES (2009): Growth dissymmetrization of rare earth element distribution and the Sm-Nd isotope system in fluorite crystals of the Nordvik deposit (Taymyr). Doklady Earth Sciences (424): 86–89.

[7] Baele, JM (1999): Reliques silicifiées et minéralisées de paléokarsts post-varisques sur le Dévonien en Belgique méridionale. Annales de la Société geologique du Nord (6): 127–133.

[8] Dickson, JAD (1980): Artificial colouration of fluorite by electron bombardment. Mineralogical magazine (43): 820–823.

[9] Marshall, DJ (1988): Cathodoluminescence of Geological Materials. Unwin Hyman, Boston: pp146.

[10] Blanc, P, Baumer, A, Cesbron, F, Ohnenstetter, D, Panczer, G, and Rémond, G (2000): Systematic cathodoluminescence spectral analysis of synthetic doped minerals: anhydrite, apatite, calcite, fluorite, scheelite and zircon. In: Pagel, M, Barbin, V, Blanc, P, and Ohnenstetter, D (editors): Cathodoluminescence in Geosciences, Springer, Berlin: 127–160.

[11] Taylor, SR and McClennan, SM (1985): The continental crust: its composition and evolution, Blackwell, Oxford: pp31.

TABLE 1: Partition coefficient $K_{|110|/|100|}$ for sample "Mat" based on analyses in coeval regions in adjacent |100| and |110| sectors in three different growth zones (six analyses in total). The dispersion is less than 15% for La to Eu and 50% for Gd to Yb.

| REE | La | Ce | Pr | Nd | Sm | Eu | Gd | Tb | Dy | Ho | Er | Tm | Yb | Lu | Y |
|---|---|---|---|---|---|---|---|---|---|---|---|---|---|---|---|
| $K_{\|110\|/\|100\|}$ | 20.4 | 16.3 | 11.7 | 8.2 | 2.5 | 1.5 | 1 | 0.74 | 0.68 | 0.69 | 0.66 | 0.70 | 0.70 | 0.73 | 0.83 |

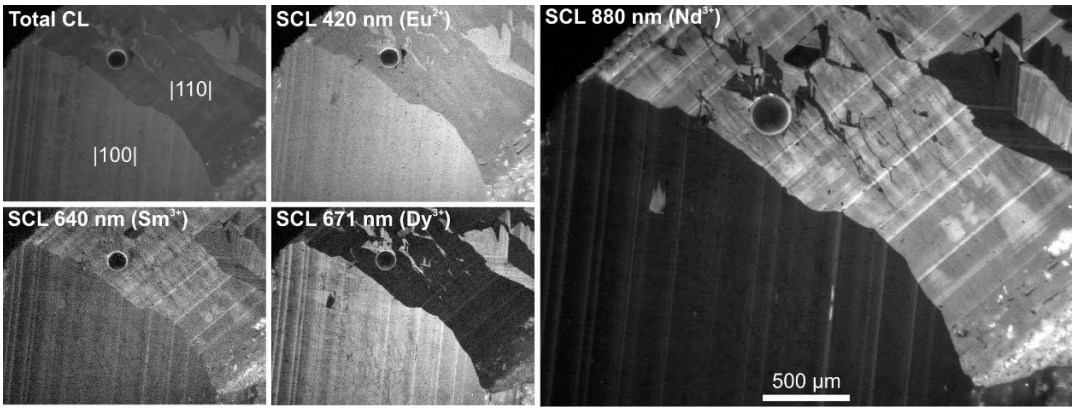


Figure 1: Total and spectral cathodoluminescence (SCL) imaging of sectorally zoned fluorite (sample "Ran"; operating conditions: 15 kV and 500 µA). The {100} and {110} crystal faces were macroscopically visible. The filtering wavelength and corresponding CL activator are indicated on top of each image. Contrast image was expanded. The dark disk is a laser ablation crater,which lies in a crystallographically heterogeneous region in the |110| sector.

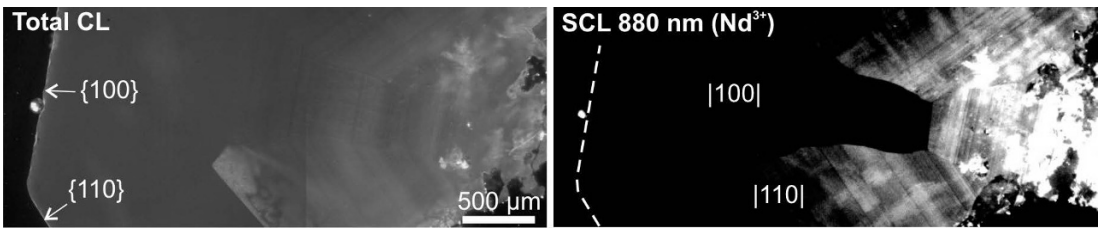


Figure 2: Total and spectral cathodoluminescence (SCL) imaging of fluorite sample "Han", showing homogeneous emission (operating conditions: 15 kV and 500 µA). Under total CL, only a faint growth zoning is visible in the central region of the crystal. Spectral imaging of the Nd emission reveals a sharp |100| and |110| sectoral zoning consistent with the macroscopically visible {100} and {110} crystal faces.

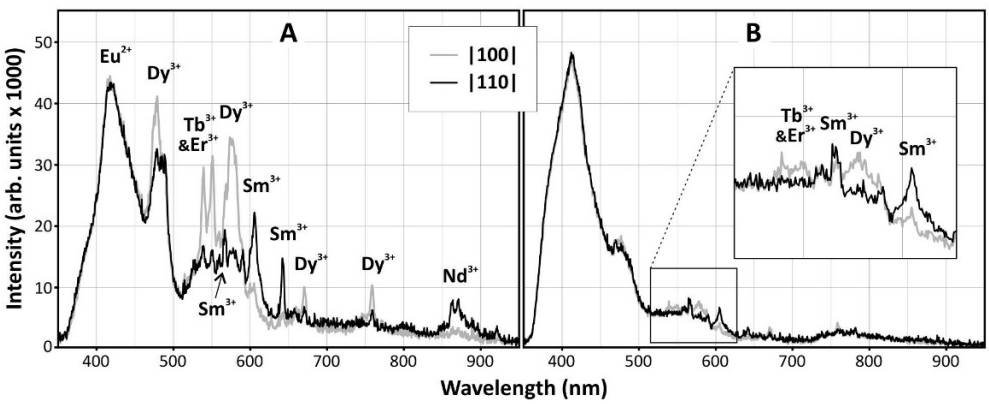


Figure 3: CL spectra in selected |100| (in grey) and |110| (in dark) sectors of fluorite from South Belgium (operating conditions: 15 kV and 500 µA). (A) Typical spectra in highly REE-activated fluorite, showing contrasting activation of HREE (Dy and Tb/Er) and LREE (Sm and Nd) in the two sectors. (B) A similar partitioning of the activators is still discernible in the spectra from weakly REE-activated fluorite, which typically exhibits homogeneous CL emission (see zoomed region in insert).

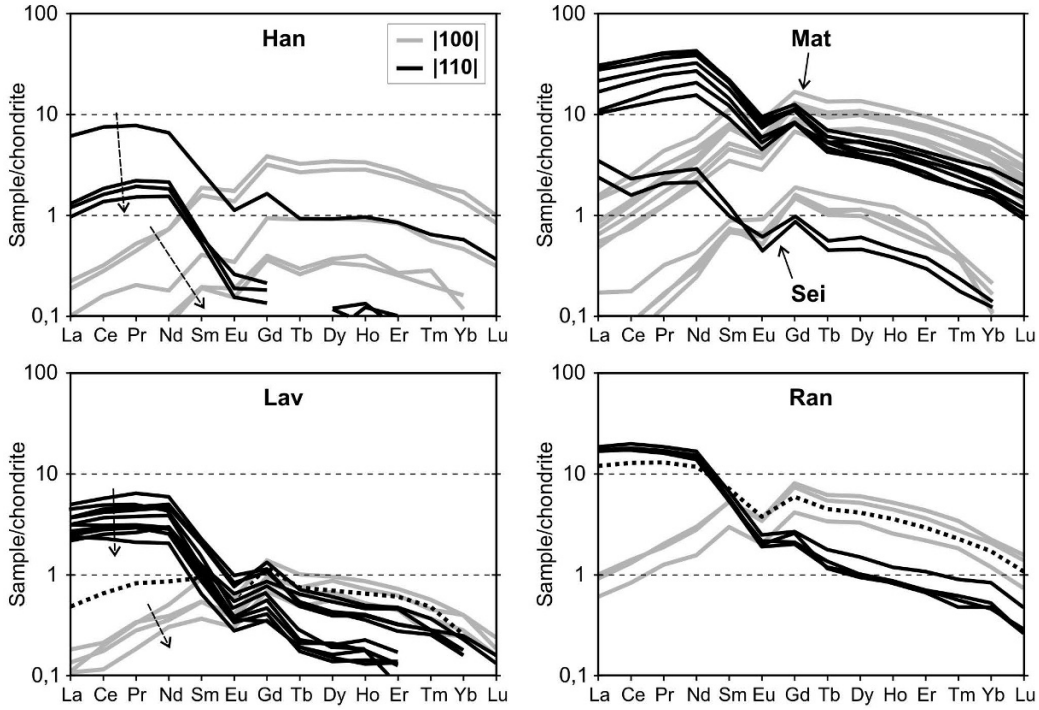


Figure 4: Chondrite-normalized REE patterns of selected samples (REE in chondrite after Taylor and McClennan [10]). The dotted patterns represent analyses in a heterogeneous, yet macroscopically visible |110| sector. Their result is therefore not representative for pure |100| or |110| sectors but a mixed influence of them (see Figure 1 for the location of spot analysis for sample "Ran"). LREE are markedly enriched and HREE depleted in the |110| sector relative to the |100| sector. Variation in LREE is 1 order of magnitude in average, which dramatically affects the shape of the patterns. The arrows indicate analyses from the centre of crystal outwards, showing a general decrease in REE concentration during crystal growth but no modification of the pattern shape.

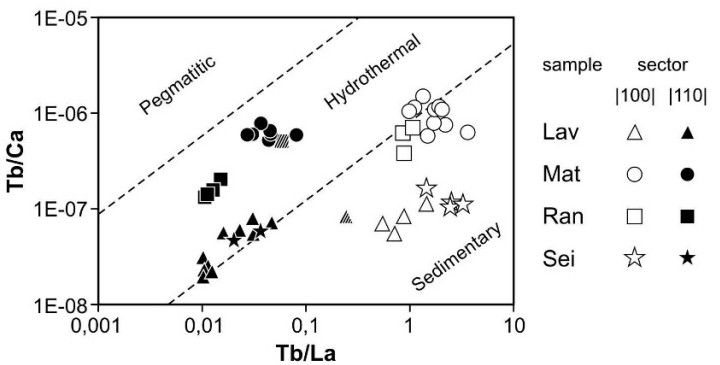


Figure 5: Tb/La-Tb/Ca diagram after [2] of five fluorite samples (two for "Mat" and one for each other) with distinction between the sectors that were analyzed (open symbols = |100| and filled symbols = |110|). The hatched symbols represent analyses in heterogeneous sectors. Note how analyses from different sectors of the same crystal plot in different fields due to variations of Tb/La of nearly 2 orders of magnitude.